Journal of Materials Chemistry A

Accepted Manuscript

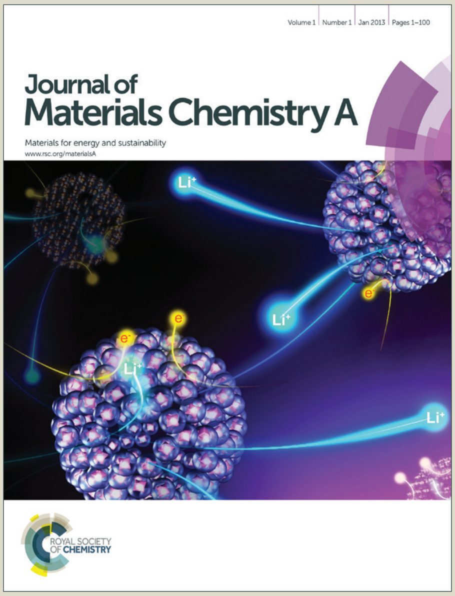

Volume 1 | Number 1 | Jan 2013 | Pages 1–100

Journal of Materials Chemistry A

Materials for energy and sustainability

www.rsc.org/materialsA

www.rsc.org/materialsA

Cite this: DOI: 10.1039/c0xx00000x

www.rsc.org/xxxxxx

ARTICLE TYPE

Oxygen Storage Capacity and Thermal Stability of $CuMnO_2$-CeO_2 Composite System

Xiubing Huang, Chengsheng Ni, Guixia Zhao and John T.S. Irvine*

Received (in XXX, XXX) Xth XXXXXXXXX 20XX, Accepted Xth XXXXXXXXX 20XX

DOI: 10.1039/b000000x

Abstract: Fast and reversible oxygen diffusion in solid oxides depending on oxygen partial pressure at low temperatures is a promising strategy for improving the overall performance and service lifetime of many energy-related materials. However, the high energy required for the redox reaction of cations and their high thermodynamic barriers have impeded the realization of fast oxygen diffusion at low temperatures. Herein, we report enhanced oxygen diffusion and storage capacity of monoclinic crednerite $CuMnO_2$ at a lower temperature by surface modification with CeO_2. The fast and reversible oxygen uptake/release can be attributed to CeO_2 that serves as fast oxygen diffusion channel between bulk $CuMnO_2$ and the surrounding atmospheres. Importantly, the amount of CeO_2 in the $CuMnO_2$-CeO_2 composite system has great effect on the total oxygen storage capacity and redox behaviour. Our findings could provide useful information for developing effective oxygen storage materials in wide energy-related applications.

1. Introduction

Solid-state oxygen storage materials (OSMs) have attracted considerable attention due to their wide applications in numerous oxygen-related energy and environmental fields, such as three-way catalysts for the effective removal of automobile exhaust emissions (e.g., NO_x, CO, and hydrocarbons).[1, 2] The development of OSMs is also crucial to the success of new energy technologies, such as oxygen enrichment to improve the efficiency of chemical looping combustion.[3] Ideal OSMs for practical applications should satisfy certain requirements and possess some properties, including large oxygen storage capacity (OSC), quick absorption/desorption of oxygen and their dependence on temperature and/or oxygen partial pressure, and good reversibility.

The most widely investigated OSMs are based on ceria (e.g., well-known $Ce_{1-x}Zr_xO_{2+\delta}$) due to the reversibly redox reaction of Ce^{3+}/Ce^{4+},[2, 4-8] however, their OSC are relatively small and usually achieved by the usage of reductive gas. Recently, Oxides based on transition metals have attracted remarkable attention due to their excellent properties, such as their flexible oxidation states, various phase structures, possible substitutions, cationic and anionic non-stoichiometry, or lattice oxygen deficient in the framework.[3, 9-13] Their oxygen storage/release behaviour is generally based on the oxygen non-stoichiometry, which can be achieved by adjusting the surrounding oxygen partial pressure (i.e., oxidative air, reductive H_2) or temperature.[11, 14] Among OSMs based on transition-metals, extensive attention has been paid to delafossite-type oxides with the general formula $CuMO_2$ (M = trivalent cation) because of the low reductive/oxidative temperature of Cu^{2+}/Cu^+, remarkable oxygen uptake ability, wide potential applications, environmental-friendliness and abundance.[15-17] However, only very limited work has been reported on the effect of trivalent cation species on the oxygen storage properties of the delafossite-type $CuMO_2$ oxides under oxidative/reductive atmospheres.[15-17] For example, Sumio Kato, et al. reported that $CuMnO_2$ and $CuFeO_2$ exhibited larger OSC values at lower temperature than those of $CuAlO_2$ and $CuGaO_2$,[15] and OSC values for x = 0.1 and 0.3 in $CuFe_{1-x}Al_xO_2$ were larger than that for x = 0 above 500 ^oC.[17] However, the full details of phase-transformation process under oxidative/inert atmospheres and effect of surface-modification by other metal oxides on the oxygen diffusion, oxygen storage capacity and thermal stability of $CuMO_2$ still remain not well-defined.

In the search for better OSMs, crednerite $CuMnO_2$ as an alternative phase to delafossite-type $CuMO_2$ seems to have great potentials due to its changeable valence and low-temperature for oxygen uptake/release,[15, 18] and its wide applications, such as hydrogen photo-evolution catalyst,[19] three-way catalyst for the removal of exhaust gases (e.g., CO, NO_x),[15] and hydrogen storage.[20] As reported by several research groups, crednerite $CuMnO_2$ exhibits the monoclinic structure at room temperature, which is consisted of edge-shared MnO_6 octahedron and two-coordinated Cu^+ cations at the interlayer sites, as represented in Figure 1.[15, 19, 21] This structure is closely related to the rhombohedral 3R delafossite structure of $CuFeO_2$ (i.e., the Cu^+ cations linearly coordinating with two O ions, and the parallel O-Cu-O chains connecting Fe^{3+} cations to form two-dimensional sheets of edge-shared FeO_6 octahedrons), but with a distortion of MnO_6 octahedron due to the Jahn-Teller effect of Mn^{3+}.[22] However, it has been reported that $Cu_{1+x}Mn_{1-x}O_2$ (0.08 < x < 0.12) at high temperature can exhibit the delafossite-like phase with hexagonal structure because the thermal expansion of the structure would result in a larger lattice distortion than that from Jahn-Teller effect.[23, 24]

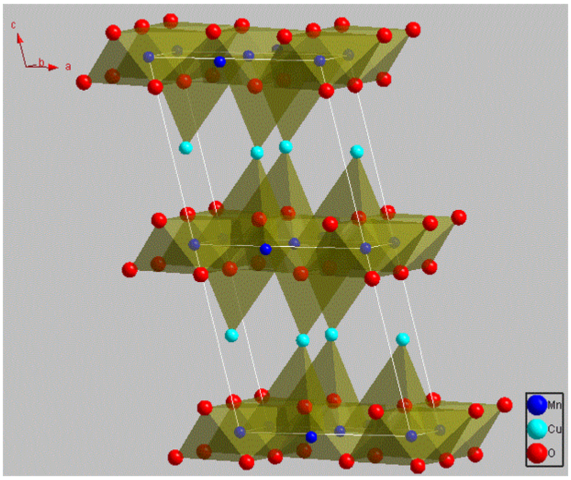

Figure 1. Schematic illustration of the crystal structure of $CuMnO_2$. The illustration was drawn with Diamond 3.1d software for crystal and molecular structure visualization.

It is well known that multiple valences of Mn cations can co-exist in many Mn-containing compounds, which could be beneficial to the oxygen-storage property.[25-27] The valence of Mn in $CuMnO_2$ has been demonstrated to be +3, however the existence of Mn^{4+} in the nonstoichiometric $Cu_{1+x}Mn_{1-x}O_2$ oxides is also detected by XPS because the excess Cu atoms would occupy the octahedral site with Cu^{2+} while the electrical neutrality principle would result in the formation of mixed Mn^{3+}/Mn^{4+}.[18, 28] In addition, the $Cu_xMn_{3-x}O_4$ spinel, one of the oxidation products of $CuMnO_2$, has been reported to show the coexistence of Mn^{3+}/Mn^{4+}, implying a possible increase in the total oxygen uptake ability under oxidative atmosphere.[27, 29, 30] However, pure crednerite $CuMnO_2$ oxide is usually synthesized using solid-state reaction at very high temperatures[15, 31, 32] or ion-exchange reaction with a long reaction time.[32] Such high reaction temperature or slow chemical conversion rate for reversible redox processes are impractical for many technological applications.[18] Therefore, it is important to improve the oxygen diffusion ability and the overall oxygen storage capacity in crednerite $CuMnO_2$ at low temperatures.

CeO_2 has been widely investigated as three-way catalysts or oxygen promoters due to the fast oxygen ionic mobility between Ce^{4+} and Ce^{3+} in reductive/oxidative atmosphere even though CeO_2 could retain its fluorite structure under oxidizing and mildly reducing atmospheres.[33-37] CeO_2 has also been reported as an interlayer or electrolyte in $La_{1-x}Sr_xCoO_{3-\delta}/CeO_2$ composite system to improve the oxygen ionic mobility, in which some chemical reactions can take place at the interfaces between perovskite and CeO_2.[38, 39] Therefore, CeO_2 may function as oxygen ionic mobility channel between oxides and their surrounding atmosphere. Here, we investigated the $CuMnO_2$-CeO_2 composite system with the purpose of further optimizing the oxygen diffusion ability and overall oxygen storage capacity at low temperatures under alternating oxidative (i.e., air or O_2) and inert (i.e., Ar) atmospheres. Modifying the surfaces of $CuMnO_2$ with CeO_2 may bring in both benefits of $CuMnO_2$ and CeO_2, thereafter adjusting their thermochemical properties (e.g., redox properties, non-stoichiometry, oxygen exchange constant, and formation of oxygen vacancies), further enhancing their OSC and thermal stability. Our research results indicate that modifying $CuMnO_2$ with a small portion of CeO_2 (e.g., the molar ratios of CeO_2 to $CuMnO_2$ smaller than 20%) can improve the oxygen storage capacity at low temperatures (< 600 °C) with a highly reversible manner.

2. Experimental Section

2.1 Sample Preparation

$CuMnO_2$-CeO_2 composites were prepared by a conventional Pechini method, followed by a solid state method. In a typical process, 10 mmol of $Cu(NO_3)_2 \cdot 2.5H_2O$ (98%) and 10 mmol of $Mn(CH_3COO)_2 \cdot 4H_2O$ (98%) were dissolved into 100 mL of deionized H_2O under continuous stirring. A certain amount (0.5, 1.0, 2.0 or 4.0 mmol) of $Ce(NO_3)_3$ $6H_2O$ (99.99%) was added into the above solution under stirring, followed by adding 20 mmol of citric acid monohydrate (99.95%) and 10 mL of ethylene glycol. After stirring for 4 h, the solvent was evaporated at 110 °C to obtain a gel. After drying, the powder was ground and pre-fired at 500 °C under static air for 1 h to get the precursor. Then the precursor was pressed into pellets and fired at 960 °C for 12 h under flowing argon. The obtained products were referred to $CuMnO_2$-xCeO_2, in which x is the molar ratio percent of CeO_2 to $CuMnO_2$ (i.e., x = mol of CeO_2/mol of $CuMnO_2$ × 100).

2.2 Characterization

Structures of all samples were characterized by X-ray powder diffraction (XRD) on a PANalytical Empyrean Reflection Diffractometer with Cu Kα irradiation (λ = 0.15418 nm). HRTEM images and TEM elemental mapping of samples were observed on a JEM-2011 Transmission Electron Microscopy (TEM) with an acceleration voltage of 200 kV equipped with an X-ray Energy Dispersive Spectroscopy (EDS). The morphologies of all samples were observed on a JEOL JSM-6700 Field Scanning Electron Microscopy (FESEM). The oxygen uptake behaviours of these samples were measured by thermogravimetric analysis (TGA) on a NETZSCH TG 209 instrument (NETZSCH-Geraetebau GmbH, Selb, Germany) with a TASC 414/3 controller. The measurements were carried out for 50 mg specimens up to 800 °C with heating rate of 10 °C/min under air or O_2 with flowing rate 25 mL/min. In addition, the reversibility of the oxygen uptake/release was carried out in the following experiments: 1) Firstly increasing temperature to 600 °C under flowing O_2 gas, then switching the gas from O_2 to Ar with temperature from 600 to 900 °C; after cooling down to 300 °C under flowing Ar, switching the gas from Ar to O_2 with temperature from 300 to 600 °C; repeated this process between 300 and 900 °C for 4 times. The thermal stability (weight and phase structure change) of as-prepared samples with temperature from room temperature to 1000 °C under flowing air was checked by TGA/DTA technique carried out on a Stanton Redcroft STA-780 series thermal analyser.

3. Results and Discussion

XRD patterns of these as-prepared $CuMnO_2$-xCeO_2 composites obtained by post-annealing at 960 °C for 12 h under flowing Ar are displayed in Figure 2. The XRD pattern for $CuMnO_2$ in Figure 2a can be indexed to a pure monoclinic structure with *C2/m* space group. All the peaks are in good agreement with the JCPDS card No. 50-0860 for the crednerite phase. For the $CuMnO_2$-xCeO_2 composites, they are obviously composed of crednerite $CuMnO_2$ and fluorite CeO_2, and no other impurity phases are observed. The XRD Rietveld refinements for $CuMnO_2$ and CeO_2 were carried out using GSAS software based on the monoclinic structure with *C2/m* space group and cubic structure with *Fm-3m* space group, respectively. The typical XRD patterns after final refinement for $CuMnO_2$ and $CuMnO_2$-40CeO_2 are shown in Figure 3, further confirming the phase composition of $CuMnO_2$ and CeO_2.[21]

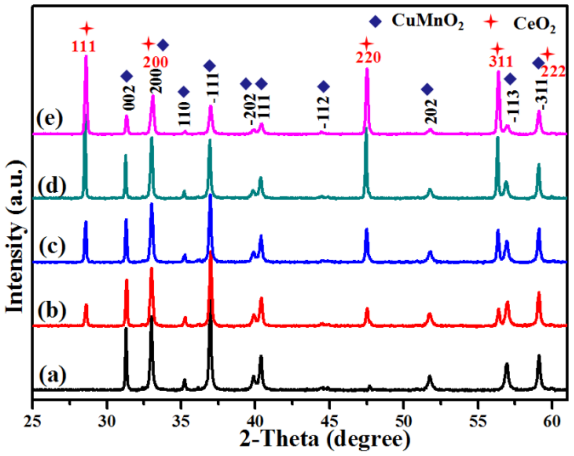

Figure 2. XRD patterns of as-prepared $CuMnO_2$-xCeO_2 (i.e., post-annealing at 960 °C under flowing Ar): (a) $CuMnO_2$, (b) $CuMnO_2$-5CeO_2, (c) $CuMnO_2$-10CeO_2, (d) $CuMnO_2$-20CeO_2, (e) $CuMnO_2$-40CeO_2.

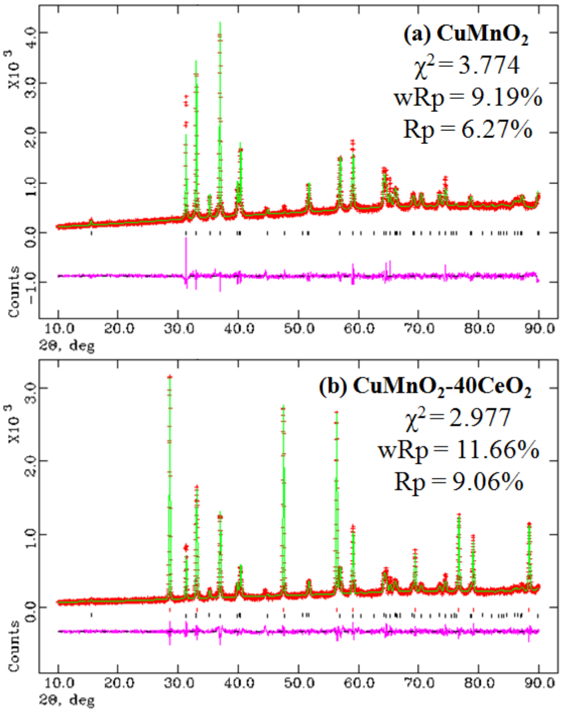

Figure 3. XRD patterns after final Rietveld refinements for as-prepared products: (a) $CuMnO_2$ and (b) $CuMnO_2$-40CeO_2.

Detailed lattice parameters for pure $CuMnO_2$ and $CuMnO_2$-xCeO_2 composites after Rietveld refinements are summarized in Table 1. There are no obvious changes in the lattice parameter *a*, *b* and *c* for $CuMnO_2$ and *a* for CeO_2 with the increasing CeO_2 amount up to x = 40 for $CuMnO_2$-xCeO_2 composite, suggesting that $CuMnO_2$ and CeO_2 exist mainly as separate phases and there may be only some contact between the surfaces. The HRTEM images of $CuMnO_2$ in $CuMnO_2$-10CeO_2 and $CuMnO_2$-40CeO_2 (Figure S1) show clear lattice fringes and these *d* spacings of 0.22 and 0.57 nm correspond to the (111) and (001) planes of $CuMnO_2$, respectively. The TEM elemental mappings of Cu, Mn, O and Ce for $CuMnO_2$-10CeO_2 (Figure S2) and $CuMnO_2$-40CeO_2 (Figure S3) also indicate the individual existence of $CuMnO_2$ and CeO_2, as well as the inhomogeneous surface contact between CeO_2 and $CuMnO_2$.

The oxygen uptake behaviours of as-prepared $CuMnO_2$-xCeO_2 composites were investigated by TGA at temperature up to 800 °C under flowing air or O_2. The results shown in Figure 4 reveal a remarkable oxygen uptake capacity of this $CuMnO_2$-xCeO_2 composite system under oxidative atmosphere, which corresponds to the following exothermic oxidation reaction:

$$CuMnO_2 + 1/(6-2y)O_2 \rightarrow 1/(3-y)Cu_yMn_{3-y}O_4 + (3-2y)/(3-y)CuO$$

(Equation 1)

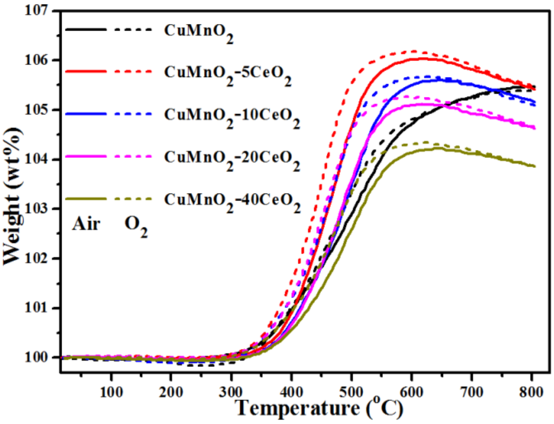

Figure 4. TGA curves of as-prepared $CuMnO_2$-xCeO_2 samples (i.e., post-annealing at 960 °C under flowing Ar for 12 h) under flowing air or pure O_2 with 25 mL/min from room temperature to 800 °C. The solid line is the TGA curves under air and the short dash is under pure O_2.

The weight for all these samples starts to increase at about 300 °C, due to the increase in the oxygen content, accompanied with the oxidation of Cu^+ and/or Mn^{3+}. Pure $CuMnO_2$ had a continuous and smooth weight increase with increasing temperature from 300 to 800 °C, reaching the maximum value of 5.475 wt% at 800 °C under both flowing air and O_2, corresponding to the formation of spinel $Cu_{1.058}Mn_{1.942}O_4$. For pure $CuMnO_2$ and $CuMnO_2$-xCeO_2 composites, the oxygen uptake rate in air is a bit slower than that in O_2 and the maximum oxygen uptake amount in air is also a bit smaller than that in O_2, in which $CuMnO_2$-5CeO_2 exhibits the most weight increase, reaching 6.169 wt% at 591 °C under flowing O_2 and 6.031 wt% at 620 °C under flowing air, respectively, suggesting higher oxygen partial pressure would enhance the oxygen uptake ability at lower temperatures. With the further increase of CeO_2 amount in the composite, the maximum OSC decreased, which can be attributed to the offset effect of CeO_2 since the weight increase is majorly

Table 1. Lattice parameters of as-prepared $CuMnO_2$-xCeO_2 obtained from Rietveld refinements by GSAS software.

As-prepared Sample	Composition	a (Å)	b (Å)	c (Å)	Cell volume (Å^3)	β
$CuMnO_2$	$CuMnO_2$	5.592(3)	2.883(1)	5.892(3)	92.1(1)	104.03(3)
$CuMnO_2$-5CeO_2	$CuMnO_2$ CeO_2	5.597(3)	2.883(1) 5.412(2)	5.892(3)	92.2(1) 158.5(2)	104.00(4)
$CuMnO_2$-10CeO_2	$CuMnO_2$ CeO_2	5.593(1)	2.883(6) 5.412(1)	5.892(1)	92.19(3) 158.5(2)	104.06(3)
$CuMnO_2$-20CeO_2	$CuMnO_2$ CeO_2	5.589(2)	2.882(1) 5.411(1)	5.891(2)	92.08(8) 158.4(1)	104.08(4)
$CuMnO_2$-40CeO_2	$CuMnO_2$ CeO_2	5.597(3)	2.883(1) 5.412(2)	5.891(3)	92.24(9) 158.5(3)	104.06(7)

caused by the oxidation of Cu^+ and/or Mn^{3+} in $CuMnO_2$ while CeO_2 could maintain its fluorite-type structure under inert atmosphere,[40, 41] as determined by XRD results in Figure 2. After reaching the maximum weight at around 600 °C, further increasing the temperature to 800 °C results in slight and smooth weight decreases (< 0.14 wt%) for all these CeO_2-modified $CuMnO_2$ samples, which can be attributed to the composition adjustment of spinel $Cu_yMn_{3-y}O_4$ with temperature.[18] These results also indicate that CeO_2-modification would favour the oxygen mobility in $CuMnO_2$ and the formation of spinel $Cu_yMn_{3-y}O_4$ with more Mn^{4+} at lower temperatures. It should be noted that the oxygen uptake in $CuMnO_2$ and $CuMnO_2$-xCeO_2 composites are mainly coming from the oxidation of $CuMnO_2$ to CuO and spinel $Cu_yMn_{3-y}O_4$. Assuming the total weight increase is only coming from the oxidation of $CuMnO_2$, the composition of spinel $Cu_yMn_{3-y}O_4$ at the maximum weight under flowing O_2 can be calculated based on **Equation 1** to be $Cu_{1.370}Mn_{1.630}O_4$ for the $CuMnO_2$-5CeO_2 starting mix, $Cu_{1.317}Mn_{1.683}O_4$ for $CuMnO_2$-10CeO_2, $Cu_{1.356}Mn_{1.644}O_4$ for $CuMnO_2$-20CeO_2 and $Cu_{1.316}Mn_{1.684}O_4$ for $CuMnO_2$-40CeO_2, while the composition of spinels at the maximum weight under flowing air can be calculated to $Cu_{1.332}Mn_{1.668}O_4$ for $CuMnO_2$-5CeO_2, $Cu_{1.296}Mn_{1.704}O_4$ for $CuMnO_2$-10CeO_2, $Cu_{1.310}Mn_{1.690}O_4$ for $CuMnO_2$-20CeO_2 and $Cu_{1.268}Mn_{1.732}O_4$ for $CuMnO_2$-40CeO_2, respectively. These calculation results suggest that higher oxygen partial pressure favour the formation of spinels with more Mn^{4+} from the oxidation of $CuMnO_2$-xCeO_2 composites.

XRD patterns of the oxygenated $CuMnO_2$ and $CuMnO_2$-xCeO_2 composites after TGA test up to 800 °C under flowing air are shown in Figure 5. While CeO_2 in these oxygenated $CuMnO_2$-xCeO_2 composites still maintained its fluorite-type cubic structure, $CuMnO_2$ was oxidized to CuO and spinel $Cu_yMn_{3-y}O_4$ oxides, in good agreement with the TGA analysis for Figure 4 and previous reported results.[18] The lattice parameters of CeO_2 and spinel $Cu_yMn_{3-y}O_4$ in the oxygenated $CuMnO_2$ and $CuMnO_2$-xCeO_2 composites after TGA test up to 800 °C in flowing air were refined from the XRD results in Figure 5 using GSAS software and summarized in Table 2. The lattice parameters of CeO_2 in the oxygenated $CuMnO_2$-xCeO_2 composites are a bit smaller than those of as-prepared $CuMnO_2$-xCeO_2 composites (as shown in Table 1), indicating the possible doping of Mn and/or Cu in the lattice of CeO_2 after oxidation. In addition, the lattice parameters of spinel $Cu_yMn_{3-y}O_4$ in the oxygenated $CuMnO_2$-xCeO_2 composites are also slightly smaller than those of oxygenated pure $CuMnO_2$, indicating the higher Cu/Mn ratios in the spinel $Cu_yMn_{3-y}O_4$ in the oxygenated $CuMnO_2$-xCeO_2 composites as the smaller ionic radii of Cu^{2+} than that of Mn^{2+} would result in lattice parameter decreases when copper ions replace manganese ions on tetrahedral sites.

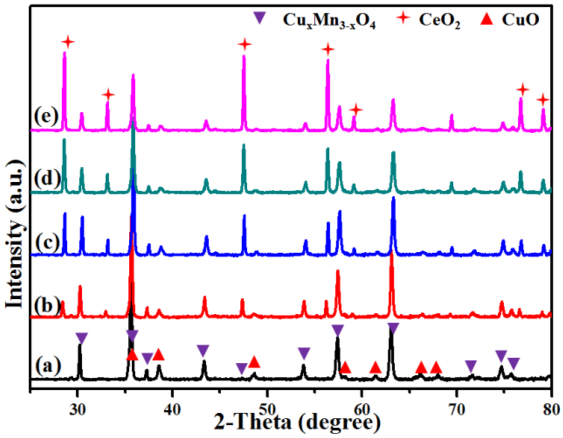

Figure 5. XRD patterns after TGA test from room temperature to 800 °C under flowing air: (a) $CuMnO_2$, (b) $CuMnO_2$-5CeO_2, (c) $CuMnO_2$-10CeO_2, (d) $CuMnO_2$-20CeO_2, (e) $CuMnO_2$-40CeO_2.

Table 2. Lattice parameters of oxygenated $CuMnO_2$-xCeO_2 in Figure 5 from Rietveld refinements by GSAS software.

Oxygenated $CuMnO_2$-xCeO_2	Composition	a (Å)	Cell volume (Å^3)
$CuMnO_2$	$Cu_yMn_{3-y}O_4$	8.317(2)	575.30(7)
$CuMnO_2$-5CeO_2	$Cu_yMn_{3-y}O_4$ CeO_2	8.307(2) 5.407(8)	573.23(4) 158.14(7)
$CuMnO_2$-10CeO_2	$Cu_yMn_{3-y}O_4$ CeO_2	8.311(5) 5.409(1)	574.06(3) 158.26(1)
$CuMnO_2$-20CeO_2	$Cu_yMn_{3-y}O_4$ CeO_2	8.309(4) 5.410(6)	573.64(9) 158.39(3)
$CuMnO_2$-40CeO_2	$Cu_yMn_{3-y}O_4$ CeO_2	8.312(2) 5.410(2)	574.27(1) 158.35(8)

To further check their thermal stability with temperature under flowing air, we treated the as-prepared samples (i.e., post-annealing at 960 °C for 12 h under flowing Ar) from room temperature up to 1000 °C with heating and cooling rates of ± 10 °C/min under flowing air, as shown in Figure 6. As discussed in aforementioned paragraphs, the as-prepared samples can start to uptake oxygen near 300 °C and reach the maximum values at near 600 °C for $CuMnO_2$-xCeO_2 composites and 800 °C for pure $CuMnO_2$, respectively. On further heating, these samples exhibit steeply weight loss from 960 °C accompanied by an endothermic peak in the DTA curves, as shown in Figure S4. Such behaviour can be attributed to the transformation of spinels and CuO back into a crednerite $Cu_{1+y'}Mn_{1-y'}O_2$ phase, accompanied with the release of O_2.[18, 32] During the cooling process under flowing air from 1000 °C, there are sharp continuous weight increases till around 880 °C, which can be attributed to the re-oxidation of crednerite phase to CuO and spinel oxides. The slight weight increase from 880 to 600 °C can be attributed to the composition adjustment of spinels with the cooling temperature, as determined by XRD shown in Figure S5. Notably, their weights at 1000 °C are higher than their pristine counterparts, suggesting CuO and spinel $Cu_yMn_{3-y}O_4$ at high temperature under air can be converted to $Cu_{1+y'}Mn_{1-y'}O_2$ rather than $CuMnO_2$ according to **Equation 2**.

$$1/(3-y)Cu_yMn_{3-y}O_4 + (3-2y)/(3-y)CuO \rightarrow \alpha Cu_{x'}Mn_{3-x'}O_4 + (2-\alpha)/2Cu_{1+y'}Mn_{1-y'}O_2 + [1/(6-2y)-\alpha/2]O_2 \qquad \textbf{(Equation 2)}$$

where $\alpha = 2y'/(3 + 3y' - 2x')$.

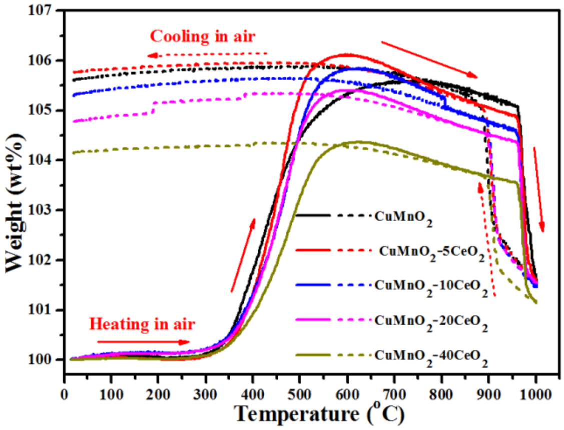

Figure 6. TGA curves of as-prepared $CuMnO_2$-$xCeO_2$ samples (i.e., post-annealing at 960 °C for 12 h under flowing Ar) from room temperature up to 1000 °C with heating and cooling rates of 10 °C/min under flowing air.

The TGA behaviours of the oxygenated $CuMnO_2$-$xCeO_2$ composites (i.e., after TGA test up to 800 °C under flowing O_2) with temperature up to 900 °C under flowing argon are displayed in Figure 7. The results show that all these samples are stable till around 600 °C under flowing argon. Further increasing temperature would lead to a continuous weight loss (< 1.2 wt%) till about 790 °C, in which the oxygenated $CuMnO_2$-$5CeO_2$ exhibited the most weight loss and the total weight loss decreased with the increase of CeO_2. The small weight loss can be attributed to the removal of oxygen in spinels. At temperatures higher than 790 °C, these sharp weight losses are attributed to the further removal of oxygen to form crednerite $Cu_{1+y'}Mn_{1-y'}O_2$.[31] To further support this conclusion, we treated the oxygenated $CuMnO_2$, $CuMnO_2$-$5CeO_2$ and $CuMnO_2$-$20CeO_2$ under flowing argon at 900 °C for 2 h and their XRD patterns shown in Figure S6 indicate the reformation of crednerite $CuMnO_2$ structure. The total weight losses for the oxygenated $CuMnO_2$-$5CeO_2$, $CuMnO_2$-$10CeO_2$ and $CuMnO_2$-$20CeO_2$ are higher than that for oxygenated $CuMnO_2$. The enhanced oxygen mobility and storage capacity in the $CuMnO_2$-$xCeO_2$ composite system can be attributed to the synergistic effect between $CuMnO_2$ and CeO_2, in which CeO_2 can act as an oxygen transfer channel or oxygen promoter dependent on temperature and/or oxygen partial pressures. The possible doping or exsolution of Cu/Mn into or from the lattice of CeO_2 on the surface dependent on the temperature and oxygen partial pressure may also contribute to the enhanced performance. Therefore, with the surface modification of CeO_2, $CuMnO_2$ can uptake oxygen from CeO_2 rather than direct from surrounding O_2 atmosphere. And vice versa, under inert Ar atmosphere, CuO and spinel $Cu_yMn_{3-y}O_4$ can release oxygen to CeO_2 lattice and then to the surroundings, rather than direct to the surroundings.

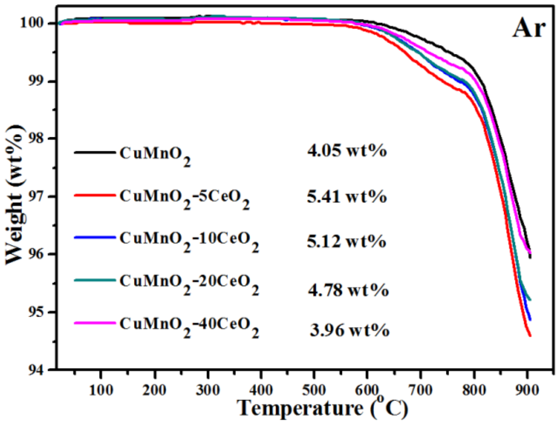

Figure 7. TGA curves of oxidized $CuMnO_2$-$xCeO_2$ samples (i.e., after TGA test up to 800 °C under flowing O_2) from room temperature to 900 °C under flowing argon with 25 mL/min.

From the TGA data in Figure 4, it appears that these CeO_2-modified $CuMnO_2$ oxides can be oxidized from 300 °C and reach the maximum weight at around 600 °C under flowing O_2, while the oxygenated samples can start to release oxygen from 600 °C under flowing argon based on the TGA results in Figure 7. These results indicate that CeO_2-modified $CuMnO_2$ oxides can cause either oxygen uptake or release depending on the temperature and/or oxygen partial pressure. Thus, remarkable oxygen uptake/release behaviours are expected via adjusting the temperature and oxygen partial pressure. As demonstrated in Figure 8, $CuMnO_2$ and CeO_2-modified $CuMnO_2$ oxides can uptake/release a large amount of oxygen in which $CuMnO_2$-$5CeO_2$ exhibits the highest OSC (ca. 6.0 wt%) and $CuMnO_2$-$20CeO_2$ shows the best reversibility under the alternating O_2 and argon between 300 and 900 °C for four cycles, indicating CeO_2 modification would improve the oxygen storage capacity as well as the reversibility of $CuMnO_2$. The OSC and reversibility would become worse with the increasing cycle times, as shown in Figure S7, but the final weight after each treatment under flowing argon during the cycles almost maintains the same, indicating that the gradual weight loss may be due to the formation of spinels with less Mn^{4+} during the oxidation process with the increasing cycling times. As shown in Figure S8, after a nine cycle test under alternating O_2 and argon, $CuMnO_2$-$5CeO_2$ still contains crednerite $CuMnO_2$ and fluorite CeO_2 phases; however, there are obvious CeO_2 nanoparticles on the $CuMnO_2$ surface, in comparison to the FESEM images in Figure S9. The TEM results for $CuMnO_2$-$10CeO_2$ after the TGA test, as shown in Figure S10, also indicate the appearance of CeO_2 nanoparticles on the surface of $CuMnO_2$, which resulted in a worse performance for the oxidation of $CuMnO_2$. The TEM elemental mapping results for $CuMnO_2$-$10CeO_2$ in Figure S10 suggest that some Cu be doped into the lattice of CeO_2 while Mn is still in $CuMnO_2$, which can be explained by the bigger ionic radius of Cu^{2+}(0.73 Å) and Cu^{+}(0.77 Å) than that of Mn^{3+} (0.58 Å) and Mn^{4+}(0.53 Å).

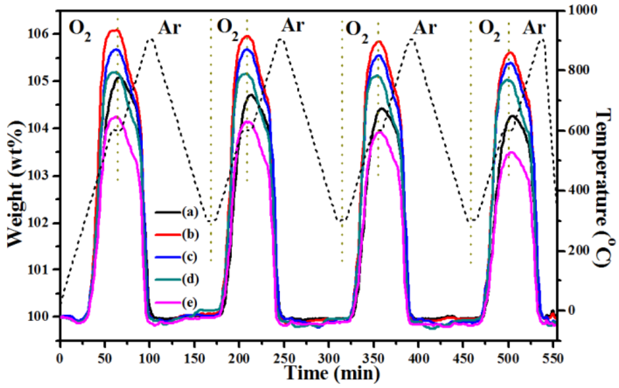

Figure 8. TGA curves of as-prepared $CuMnO_2$-$xCeO_2$ samples (i.e., post-annealing at 960 °C for 12 h under flowing Ar) under alternating O_2 and argon. The samples were firstly oxidized under O_2 to 600 °C, then switched the gas to argon and increased the temperature to 900 °C. After cooled down to 300 °C under argon, the gas was then switched back to O_2 and oxidized to 600 °C.

4. Conclusions

In conclusion, we found that fast and reversible oxygen mobility, and increased oxygen storage capacity in crednerite $CuMnO_2$ could be achieved at reduced temperatures (ca. 600 °C) by surface modification with CeO_2 in an amount less than 20 mol% in the $CuMnO_2$-CeO_2 composite system. The fast and reversible oxygen uptake/release and increased oxygen storage capacity at lower temperatures can be attributed to the synergistic effect of CeO_2 as oxygen diffusion channel between bulk $CuMnO_2$ and the surrounding atmospheres, favouring the reversible formation of spinels at lower temperatures. Our findings reported here could provide a pathway for the design and developing effective oxygen storage materials in a range of energy-synergetic related applications at low temperatures.

Acknowledgements

The authors gratefully thank the Engineering and Physical Sciences Research Council (EPSRC) platform grant EP/I022570/1 and EP/I022570/2 for financial support.

Notes and references

School of Chemistry, University of St Andrews, St Andrews, Fife, UK: Fax: +44(0)1334463808; Tel: +44(0)133463680; Email: jtsi@st-andrews.ac.uk.

† Electronic Supplementary Information (ESI) available: Additional XRD, TGA/DTA, HRTEM and FESEM images as well as TEM elemental mappings. See DOI: 10.1039/b000000x/

1. H. C. Yao and Y. F. Y. Yao, *J. Catal.*, 1984, **86**, 254-265.
2. C. E. Hori, H. Permana, K. Y. S. Ng, A. Brenner, K. More, K. M. Rahmoeller and D. Belton, *Appl. Catal. B-Environ.*, 1998, **16**, 105-117.
3. T. Motohashi, Y. Hirano, Y. Masubuchi, K. Oshima, T. Setoyama and S. Kikkawa, *Chem. Mater.*, 2013, **25**, 372-377.
4. M. Ozawa, M. Kimura and A. Isogai, *J. Alloys Compd.*, 1993, **193**, 73-75.
5. A. Gupta, U. V. Waghmare and M. S. Hegde, *Chem. Mater.*, 2010, **22**, 5184-5198.
6. M. P. Yeste, J. C. Hernandez-Garrido, D. C. Arias, G. Blanco, J. M. Rodriguez-Izquierdo, J. M. Pintado, S. Bernal, J. A. Perez-Omil and J. J. Calvino, *J. Mater. Chem. A*, 2013, **1**, 4836-4844.
7. X. Wang, G. Lu, Y. Guo, L. Jiang, Y. Guo and C. Li, *J. Mater. Sci.*, 2009, **44**, 1294-1301.
8. Q. Dong, S. Yin, C. Guo, T. Kimura and T. Sato, *RSC Advances*, 2012, **2**, 12770-12774.
9. S. Remsen and B. Dabrowski, *Chem. Mater.*, 2011, **23**, 3818-3827.
10. O. Parkkima, H. Yamauchi and M. Karppinen, *Chem. Mater.*, 2013, **25**, 599-604.
11. S. Carter, A. Selcuk, R. J. Chater, J. Kajda, J. A. Kilner and B. C. H. Steele, *Solid State Ionics*, 1992, **53–56, Part 1**, 597-605.
12. M. Cherry, M. S. Islam and C. R. A. Catlow, *J. Solid State Chem.*, 1995, **118**, 125-132.
13. J. W. Lekse, S. Natesakhawat, D. Alfonso and C. Matranga, *J. Mater. Chem. A*, 2014, **2**, 2397-2404.
14. H. Jeen, W. S. Choi, M. D. Biegalski, C. M. Folkman, I. C. Tung, D. D. Fong, J. W. Freeland, D. Shin, H. Ohta, M. F. Chisholm and H. N. Lee, *Nat. Mater.*, 2013, **12**, 1057-1063.
15. S. Kato, R. Fujimaki, M. Ogasawara, T. Wakabayashi, Y. Nakahara and S. Nakata, *Appl. Catal. B-Environ.*, 2009, **89**, 183-188.
16. S. Kato, H. Sato, M. Ogasawara, T. Wakabayashi, Y. Nakahara and S. Nakata, *Solid State Sci.*, 2012, **14**, 177-181.
17. S. Kato, S. Suzuki, R. Kawashima, M. Ogasawara, T. Wakabayashi, Y. Nakahara and S. Nakata, *J. Mater. Sci.*, 2013, **48**, 8077-8083.
18. M. Trari, J. Töpfer, P. Dordor, J. C. Grenier, M. Pouchard and J. P. Doumerc, *J. Solid State Chem.*, 2005, **178**, 2751-2758.
19. Y. Bessekhouad, M. Trari and J. P. Doumerc, *Int. J. Hydrogen Energ.*, 2003, **28**, 43-48.
20. S. A. M. Abdel-Hameed, F. H. Margha and A. A. El-Meligi, *Int. J. Energ. Res.*, 2014, **38**, 459-465.
21. Y. Bessekhouad, Y. Gabes, A. Bouguelia and M. Trari, *J. Mater. Sci.*, 2007, **42**, 6469-6476.
22. J. Topfer, M. Trari, P. Gravereau, J. P. Chaminade and J. P. Doumerc, *Z. Kristallogr.*, 1995, **210**, 184-187.
23. Driessne.Fc and G. D. Rieck, *Z. Anorg. Allg. Chem.*, 1967, **351**, 48-62.
24. Driessne.Fc and G. D. Rieck, *Zeitschrift Fur Anorganische Und Allgemeine Chemie*, 1967, **351**, 48-&.
25. J. Li, S. Xiong, X. Li and Y. Qian, *Nanoscale*, 2013, **5**, 2045-2054.
26. N. K. Radhakrishnan and A. B. Biswas, *Phys. Status Solidi A*, 1977, **44**, 45-49.
27. D. P. Shoemaker, J. Li and R. Seshadri, *J. Am. Chem. Soc.*, 2009, **131**, 11450-11457.
28. H. Y. Chen and D. J. Hsu, *J. Alloys Compd.*, 2014, **598**, 23-26.
29. I. N. Dubrovina, V. F. Balakirev and A. V. Antonov, *Inorg. Mater.*, 2001, **37**, 76-81.
30. E. Ríos, S. Abarca, P. Daccarett, H. Nguyen Cong, D. Martel, J. F. Marco, J. R. Gancedo and J. L. Gautier, *Int. J. Hydrogen Energ.*, 2008, **33**, 4945-4954.
31. A. P. Amrute, Z. Łodziana, C. Mondelli, F. Krumeich and J. Pérez-Ramírez, *Chem. Mater.*, 2013, **25**, 4423-4435.
32. B. Bellal, B. Hadjarab, N. Benreguia, Y. Bessekhouad and M. Trari, *J. Appl. Electrochem.*, 2011, **41**, 867-872.
33. Z. Liu, Z. Wu, X. Peng, A. Binder, S. Chai and S. Dai, *J. Phys. Chem. C*, 2014, **118**, 27870-27877.
34. L. Shi, W. Chu, F. Qu and S. Luo, *Catal. Lett.*, 2007, **113**, 59-64.
35. A. Hornés, A. B. Hungría, P. Bera, A. L. Cámara, M. Fernández-García, A. Martínez-Arias, L. Barrio, M. Estrella, G. Zhou, J. J. Fonseca, J. C. Hanson and J. A. Rodriguez, *J. Am. Chem. Soc.*, 2009, **132**, 34-35.
36. S. D. Senanayake, D. Stacchiola and J. A. Rodriguez, *Acc. Chem. Res.*, 2013, **46**, 1702-1711.
37. I. Moog, C. Feral-Martin, M. Duttine, A. Wattiaux, C. Prestipino, S. Figueroa, J. Majimel and A. Demourgues, *J. Mater. Chem. A*, 2014, **2**, 20402-20414.
38. E. Y. Konysheva, S. M. Francis, J. T. S. Irvine, A. Rolle and R.-N. Vannier, *J. Mater. Chem.*, 2011, **21**, 15511-15520.
39. E. Konysheva, R. Blackley and J. T. S. Irvine, *Chem. Mater.*, 2010, **22**, 4700-4711.
40. A. S. Ivanova, *Kinet. Catal.*, 2009, **50**, 797-815.
41. Y. Zhou and M. N. Rahaman, *Acta Mater.*, 1997, **45**, 3635-3639.

Fast oxygen diffusion and improved oxygen storage capacity in crednerite $CuMnO_2$ have been achieved at reduced temperatures by surface modification with CeO_2.

TOC: